ADVANCED ENGINEERING MATERIALS

FULL PAPER

DOI: 10.1002/adem.201300430

Investigation of the Thin-Film Phase Diagram of the Cr–Ni–Re System by High-Throughput Experimentation**

By *Amin Janghorban, Janine Pfetzing-Micklich, Jan Frenzel* and *Alfred Ludwig**

The Cr–Ni–Re system was investigated over the whole composition range using combinatorial fabrication methods combined with high-throughput characterization techniques in order to establish its thin film phase diagram. After annealing at 940 and 1100 °C, the phase equilibrium was reached in the Ni-rich part of the ternary in agreement with the published bulk phase diagram. Annealing the materials library at 940 °C is not sufficient to achieve the equilibrium state in the Re-rich part of the system, however by annealing the materials library at 1100 °C the formation of expected phases (three solid-solutions and a topologically close packed compound) could be observed. As a result of this study, a thin film phase diagram of the complete Cr–Ni–Re at 1100 °C was established, which is well comparable to the bulk phase diagram. This shows that the combinatorial thin film phase diagram approach is feasible and especially promising for materials systems with expensive and/or high melting point constituents.

1. Introduction

Ni-based superalloys are used in turbine blades of aero-engines and stationary gas turbines because of their good high temperature mechanical and creep properties as well as their resistance to chemical decomposition.[1–3] Among the alloying elements used in Ni-based superalloys, Re is one of the key additives to improve the mechanical properties at high temperatures.[4,5] In as-received superalloys, which are generally not in the equilibrium state, Re is supersaturated in the matrix. During service at elevated temperatures, the alloy approaches its equilibrium state where Re can contribute to the formation of undesirable brittle topologically close packed (TCP) phases such as σ, R, μ, and R phases.[6] The formation of TCP phases leads to some undesirable effects, i.e. needle-shaped precipitates of TCP phases and depletion of Re from the γ/γ' microstructure which is associated with a reduction in creep resistance.[7]

In order to avoid the formation of TCP phases, one has to rely on thermodynamic data that are valid at the service temperature. Although the formation of TCP phases in superalloys is undesired, Narita found that the ternary Cr–Ni–Re σ-phase is a good candidate as a diffusion barrier layer between Ni-based superalloys and thermal barrier coatings.[8] So far, only a few experimental works were realized with the aim of investigating the Cr–Ni–Re system by means of diffusion couples[9] and tie-line compositional analysis in the Al–Cr–Ni–Re quaternary system.[10] The experimental techniques used in these works show clearly the difficulties in investigation and development of alloy systems containing refractory metals like Re and W. This is related to their high melting temperature and the long-range diffusion paths needed to reach the equilibrium state. As alloying elements like Re are rare and expensive, studying such alloy systems over the whole composition area is highly cost consuming.

Thin-film combinatorial materials science is an efficient and economical approach for the investigation of alloy systems over complete binary and ternary as well as large composition ranges in quaternary systems.[11] Moreover, using thin-film methods minimizes consumption of expensive elements such as Re. Furthermore, as the critical diffusion length to reach the equilibrium state in thin films is significantly shorter than in bulk materials, i.e. nanometer versus micrometer, the required annealing time is much shorter and thus the equilibrium state can be achieved faster.

In this work, we use thin-film combinatorial/high-throughput techniques to study the phase equilibria in the complete ternary Cr–Ni–Re system. The present work is relevant for the establishment of phase diagrams, especially for superalloy subsystems as well as for other systems containing rare and expensive elements and/or elements with low diffusion rates.

[*] *A. Janghorban, J. Pfetzing-Micklich, J. Frenzel, A. Ludwig*
Ruhr-University Bochum, Institute for Materials, 44780 Bochum, Germany
E-mail: alfred.ludwig@rub.de

[**] *This work was supported by the German Research Foundation (DFG) through project B5 in the framework of SFB/Transregio 103.*

ADVANCED ENGINEERING MATERIALS

Table 1. Sputter conditions used for fabrication of materials libraries.

Elemental target	Supplier	Purity	Direct current density [W cm^{-2}]	Deposition rate [nm s^{-1}]
Cr	FHR	99.97	0.89	0.25
Ni	KJ Lesker	99.995	1.27	0.25
Re	KJ Lesker	99.99	1.27	0.24

Table 2. Annealing conditions for the two materials libraries.

	Temperature [°C]	Time [h]	Atmosphere		
				Pressure [kPa]	Gas flow [sccm]
ML1/940	940	36	Ar	0.002	15
ML2/1100	1100	2	He	102	200

2. Experimental Details

Thin films were deposited on 100 mm diameter polycrystalline Al_2O_3 substrates by magnetron sputtering from 4 inch diameter Cr, Ni and Re targets. The sputter conditions are listed in Table 1. The chamber base pressure was 5×10^{-7} Pa, the Ar deposition pressure was 0.3 Pa and the Ar flow rate during deposition was 10 sccm. Deposition was performed onto a heated substrate at 300 °C.

The ternary continuous composition spread type thin film materials libraries were fabricated by a wedge-type multilayer technique by successive deposition of 270 nanoscale wedge-type elemental layers, see Figure 1. The substrate was not masked in order to obtain all compositions of the ternary system. The wedge-type layers were made using a moving shutter, which was set to shield the substrate and then was slowly retracted during deposition. This leads to the formation of a single wedge-type layer with a nominal linear thickness variation from 0 to 7 nm. Ternary composition spreads were realized by rotating the substrate by 120° each time before the deposition of the next elemental layer. For achieving the fabrication of the complete ternary system and the three binary systems on a single substrate, the movement of the shutter was stopped at an intermediate position, and thus the length of the wedge-type layer was intentionally limited to 73 mm. The total film thickness, as estimated from the individual sputter rates, was about 600 nm.

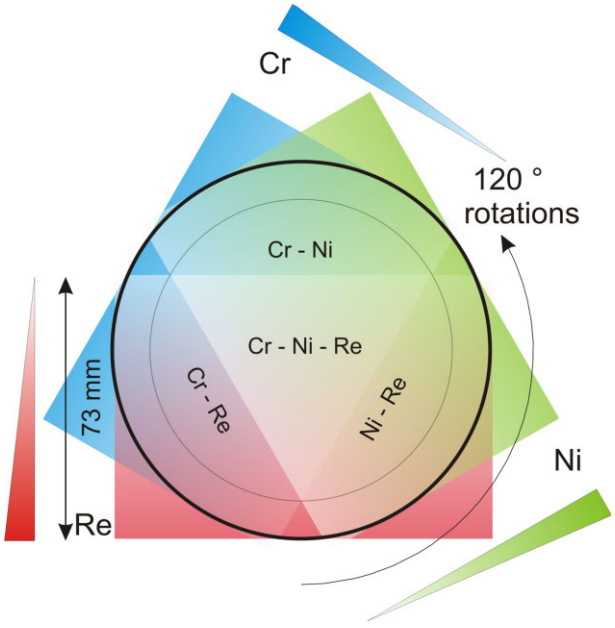

Fig. 1. Schematic of the fabrication process for the synthesis of a continuous composition spread materials library[11,23] containing the whole Cr–Ni–Re system, as well as the three binaries (an animated movie of the sputter deposition scheme for the fabrication of ternary materials libraries is available at www.rub.de/wdm).

Two materials libraries were fabricated in the aim of investigating the effect of annealing temperature on phase crystallization and on phase equilibrium. By annealing the materials library, which consists in the as deposited state of a $(Cr/Ni/Re)_{90}$ multilayer, should transform into alloy(s). The first materials library (ML1/940) was annealed directly after the deposition at 940 °C (the chamber temperature limit) for 36 h under flowing Ar (see Table 2) in the sputter chamber. The second materials library (ML2/1100) was cut into four pieces, which were then annealed in a tube furnace at 1100 °C for 2 h under a He atmosphere with a slight overpressure. The annealing conditions for the two materials libraries are listed in Table 2.

The compositions being present on the thin-film materials libraries were measured by an automated EDX method using a JEOL 5800LV SEM equipped with an Oxford INCA EDX system. A measurement grid of 342 measurement areas with an x, y step increment of 4.5 mm was used.

Automated XRD measurements using Bragg–Brentano geometry were used to analyze the coexisting phases as a function of the composition. The experiments were carried out at room temperature using a PANalytical X'Pert PRO MRD (X'Celerator detector, Cu Kα radiation, 2θ-range: 30° to 85°, spot size 3 mm × 5 mm). Due to the spot size of the XRD system, the XRD measurement area averages across a compositional space between 4 and 7 at%.

3. Results and Discussion

Figure 2 shows the results from EDX measurements in 342 measurement areas on ML2/1100 indicating the distribution of the constituent elements over the materials library after annealing. The compositional gradients over the substrate are visualized by color-coding. The Cr, Ni, and Re contents range from 0 to 96 at%, from 1 to 99 at%, and from 0 to 84 at%, respectively.

Figure 3 shows the measured compositions in the ternary plot for the two materials libraries after annealing. The compositions on ML1/940 cover the whole ternary composition range and also the three binary parts. In ML2/1100, the

FULL PAPER

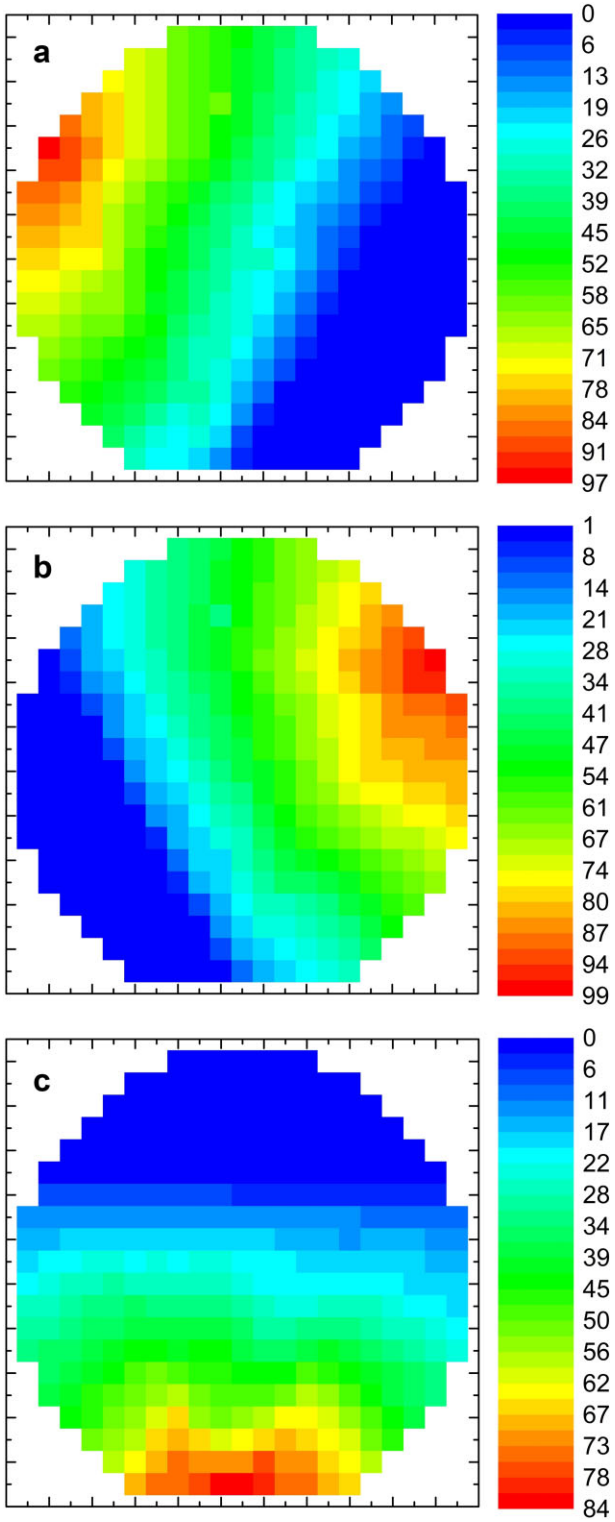

Fig. 2. EDX analysis of Cr–Ni–Re continuous thin-film composition spreads for the materials library annealed at 1100 °C (ML2/1100). (a) Cr–, (b) Ni–, (c) Re– distribution in at% over the substrate.

measured compositions cover as well the complete ternary composition space.

From the XRD patterns of the 342 analyzed points on ML2/1100, the formation of three solid-solutions (Cr), (Ni), and (Re),

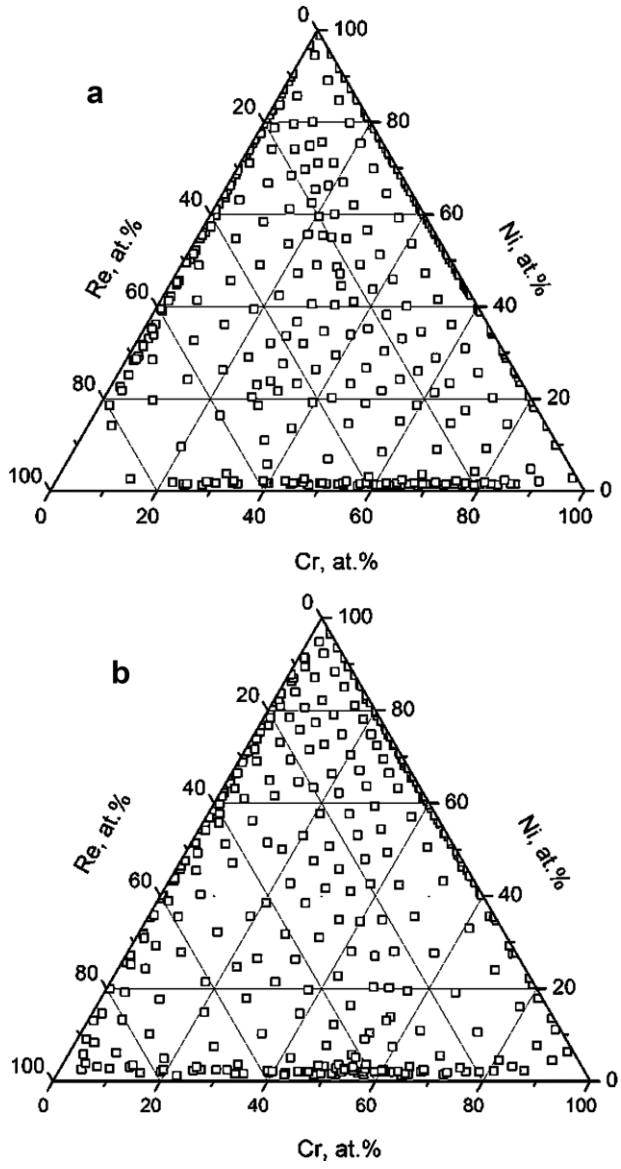

Fig. 3. Ternary composition diagram for (a) ML2/1100 (b) ML1/940. □ symbols indicate the measured compositions.

and the formation of the σ-phase were observed by comparison of the measured peak positions with those according to literature.[9] Concerning ML1/940, the XRD patterns show that the phase equilibrium was not reached in the Re-rich part and in the Cr–Re binary part of the system.

Vegard's law[12] was used to estimate the borders of the solid solutions. Applying this rule requires a certain number of samples in the single-phase solid-solution area and also in the neighboring two-phase area. Moreover, it should be only applied in a binary or a pseudo-binary composition range. The influence of thin film stresses was neglected, as it was assumed that the stress levels of neighboring compositions should be quite similar. As the solubility of Ni in both Cr and Re at 940 and 1100 °C, the solubility of Cr in Re at 940 and 1100 °C and the solubility of Re in Ni at 940 °C is < 10%, they could not be investigated by Vegard's law due to the lack of points on the

ADVANCED ENGINEERING MATERIALS

materials library in the mentioned single-phase solid-solution areas. As the crystallinity of Cr solid solution was low in the ML1/940, it was not possible to determine the position of the diffraction peaks with high precision. Therefore, Vegard's law was used to estimate the solubility of Cr in Ni at both temperatures and the solubility of Re in Ni only at 1100 °C. As Ni_{111} and Cr_{110} diffractions appear at the same 2Θ value, the (*200*) diffraction of Ni was used to determine the solubility of Cr in Ni. Figure 4a and b show the measured values of the (*200*) d-spacings in the Ni solid solution as a function of the Cr content. The solubility limits determined for the materials libraries annealed at 940 and 1100 °C are 46 and 48%, respectively. Figure 4c shows the values of the (*111*) d-spacings in Ni solid-solution as a function of the Re content in the Ni–Re binary part of the system annealed at 1100 °C. The solubility limit of Re in Ni is estimated to be 16%. These solubility limits are in good agreement with experimental values from bulk samples and with theoretical data. Udovskii *et al.*[13] reported experimental solubility limits for Ni–Cr as 44% (940 °C) and 49% (1100 °C), and Turchi *et al.*[14] calculated limits of 43 and 48%, respectively. For the Ni–Re solid solutions Nash *et al.* performed experimental and theoretical investigations. From their experiments they found a solubility limit of 14%,[15] whereas their calculations gave a limit of only 6%.[16]

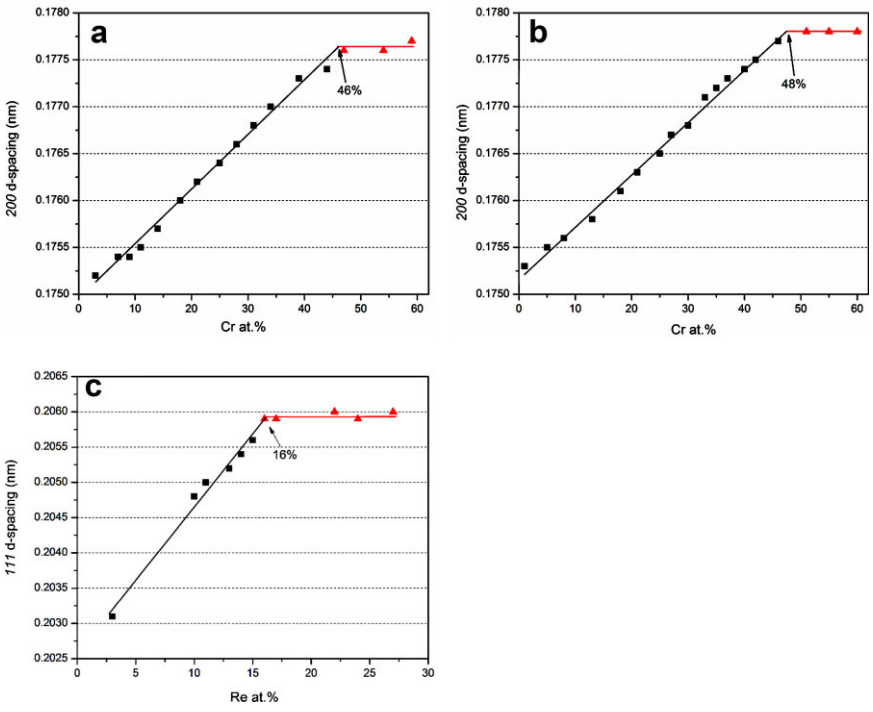

Fig. 4. Room temperature values of the (200) d-spacing of Ni solid-solution versus Cr at% for (a) ML1/940 and (b) ML2/1100. (c) Room temperature (111) d-spacings of Ni solid solution versus Re at% for ML2/1100. The intersection between the trend line for the values in the single-phase area (black line) and the one for the values in the two-phase area (red line) shows the solubility limit of Cr in Ni and Re in Ni, respectively.

The only compound that is formed in the system is the binary Cr_2Re_3 σ-phase with a wide homogeneity domain in the binary part of the system.[17,18] By substituting Ni atoms, the binary homogeneity domain spreads in the ternary composition range and covers ~7% of the phase diagram (at 1150 °C).[9]

Figure 5 compares the XRD patterns taken from the measurement regions with the composition of $Cr_{40}Ni_2Re_{58}$ from ML1/940 and ML2/1100 to the one calculated by PowderCell software[19] using the refined crystallographic data reported by Tuganbaev *et al.*[20] The position of the reflections from the measured point on ML2/1100 matches the position of the calculated reflections. The XRD pattern of the measured point on ML1/940 shows a few weak and humped reflections due to poorly-crystallized phase. Besides, the presence of a strong peak according to the formation of Re solid solution at $2\Theta = 40.5°$ shows that the phase equilibrium was not achieved in the Re-rich part of the materials library annealed at 940 °C.

The XRD patterns from the 342 measurement areas on ML2/1100 were studied individually to identify the phases formed corresponding to each composition. These phases are mapped as function of composition in Figure 6. Based on the phase mapping, the thin-film phase diagram of the system at 1100 °C is drawn as shown in Figure 7a. The illustrated boundaries between different areas on the diagram were drawn approximately, due to the limited resolution of the XRD

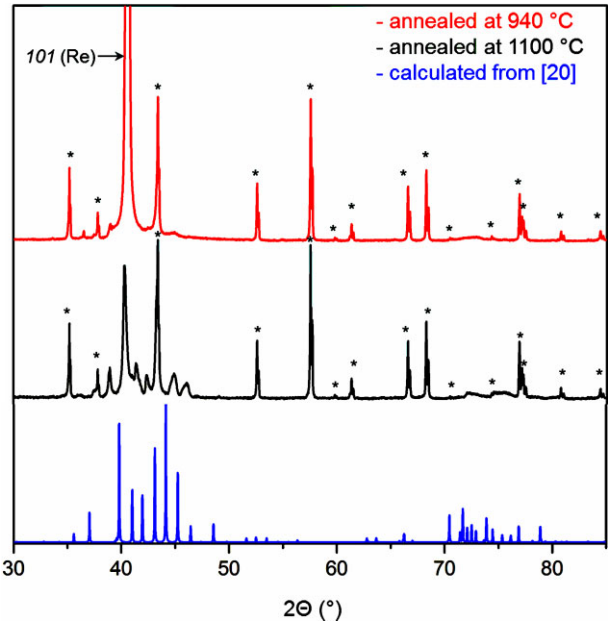

Fig. 5. XRD patterns of the measured points with a quasi-binary composition of $Cr_{40}Ni_2Re_{58}$ from ML1/940 and ML2/1100 compared to the calculated one. Reflections indicated by (*) belong to the polycrystalline Al_2O_3 substrate.

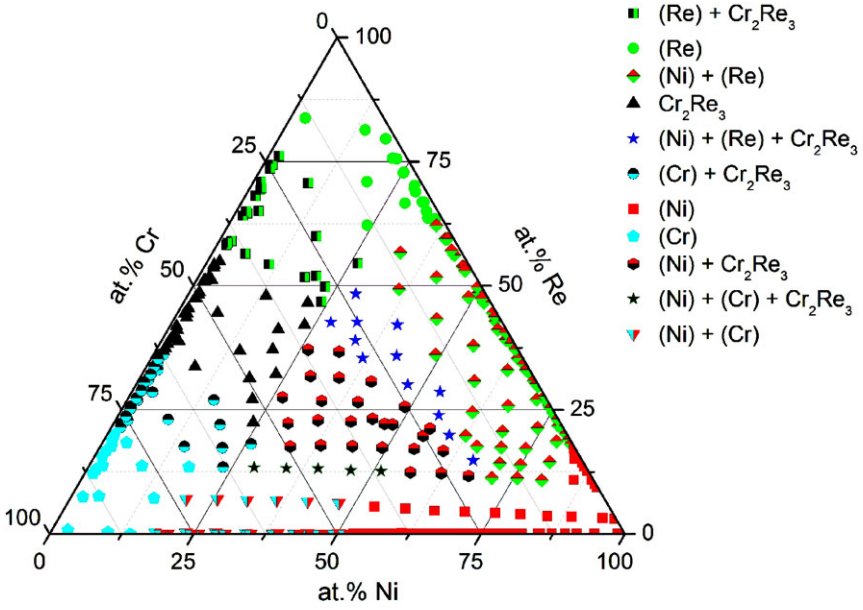

Fig. 6. Phase map of the thin-film system Cr–Ni–Re annealed at 1100 °C for 2 h.

analysis, to respect the phase diagram rules. Figure 7b shows the reported phase diagram of the system at 1150 °C for bulk samples.[9]

Comparing these two-phase diagrams, the composition range of the homogeneity domain of Ni solid solution is similar. In the binary parts the limits of Ni solid-solution are in agreement with the values obtained using Vegard's law (Figure 4) which are also close to the ones reported for the bulk samples in literature.[9,13–15]

Concerning Cr solid-solution, even though the solubility of Ni in Cr in the binary part is close to the value reported for bulk samples,[9] the solubility of Re in Cr in the binary part is smaller. Besides, in the thin-film phase diagram the Re solubility in the ternary composition area shows no significant change by variation of Ni content and the Ni solubility in the ternary composition area increases by increasing Re content. However, in the phase diagram for bulk materials, both Re and Ni solubility in Cr decrease when Ni content and Re content are increasing, respectively.

Concerning Re solid solution in the thin film phase diagram, again the solubility of Ni in Re in the binary part is close to the value reported for bulk samples[9] but the solubility of Cr in Re is much higher both in the Re–Cr binary part and in the related ternary composition area. This can be explained by comparing Re atomic radius, 138 pm, to Cr atomic radius, 128 pm.[21]

The Cr_2Re_3 compound shows a wide homogeneity domain in the Cr–Re binary area, from 40 up to 63 at% Cr. This homogeneity domain is much wider than the ones reported in the bulk samples, i.e. 37–48 at%,[9] 34–44 at%,[17] and 38–50 at %.[18] The homogeneity domain of the compound in the thin-film phase diagram extends up to 25 at% Ni in the ternary composition area which is close to 21 at% reported for the bulk samples (Figure 7b).

4. Conclusions

Thin film materials libraries covering the whole ternary Cr–Ni–Re composition were fabricated by combinatorial magnetron sputtering. After annealing at 940 °C (36 h) and 1100 °C (2 h) the materials libraries were characterized by high-throughput EDX and XRD techniques. In both materials libraries the formation of the three solid solutions was observed according to the literature. The Cr_2Re_3 intermetallic compound was formed in the materials library annealed at 1100 °C, but the compound formation was not confirmed after annealing at 940 °C which should be due to the effect of temperature on the crystallization of the complex phase.

The phase diagram of the Cr–Ni–Re system at 1100 °C has been drawn based on the identified phases from XRD analysis

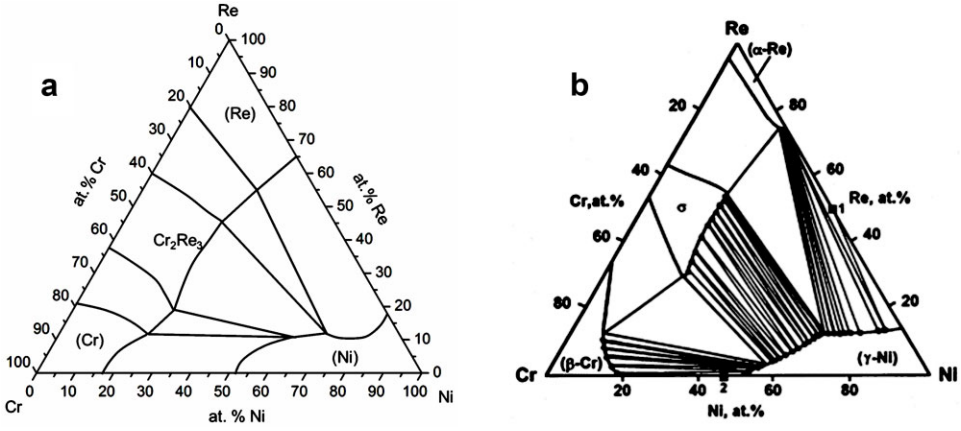

Fig. 7. (a) Thin-film phase diagram of Cr–Ni–Re system at 1100 °C. (b) Phase diagram of the system at 1150 °C for bulk materials as reported in ref.[9]

ADVANCED ENGINEERING MATERIALS

and is in good agreement, especially in the Ni-rich part, with the already published phase diagram of the system at 1152 °C for bulk materials. The main difference between the two phase diagrams concerns the shape of Cr solid-solution and Re solid-solution areas. These differences could be due:

1. The XRD spot size (3 mm × 5 mm) used in high-throughput analysis in this study is much bigger than the one used in high-throughput EDX measurements, which reduces the resolution of phase identification. In the zones on the composition diagram (Figure 3a) within the lower density of the measured points, the composition gradient in the XRD measured area could be the source of an error; especially for the points close to phase boundaries. If a higher resolution of the phase identification after a first screening is necessary, these measurements have to be carried out at a synchrotron source.
2. In compositional areas were multiple phases are present, when the amount of one phase is much lower than the other phases, it is difficult to identify the presence of the minor phase from XRD measurements. This is the main error source in this work for defining the exact positions of the phase boundaries.
3. If the assumption of similar stress levels for neighboring compositions would not hold, the limits of solid solutions could be shifted. To clarify this, a high-throughput study of stresses in the ternary system[22] would be necessary.
4. The phase diagram for bulk materials[9] is based on the compositional study of $Cr_{0.54}Ni_{0.46}/Ni_{0.50}Re_{0.50}$ diffusion couple. The few number of points studied in ref.[9] could be an error source concerning the bulk phase diagram.

Despite the differences observed between the thin film and the bulk phase diagrams, this work shows that the combinatorial thin film method is a promising technique to investigate high temperature ternary systems; especially the ones which have not been well studied due to the diffusion problem of refractory metals and/or the expenses of some particular elements which make it costly to study the system over its whole composition range.

Received: September 5, 2013
Final Version: October 22, 2013
Published online: December 27, 2013

[1] Z. Huda, P. Edi, *Mater. Des.* **2013**, *46*, 552.
[2] C. T. Sims, N. S. Stoloff, W. C. Hagel, (Eds: *Superalloys II: High Temperature Materials for Aerospace and Industrial Power*, 2nd Edn. WileyBlackwell, New York **1987**.
[3] R. C. Reed, K. A. Green, P. Caron, T. P. Gabb, M. G. Fahrmann, E. S. Huron, S. A. Woodard, *Superalloys 2008*, John Wiley & Sons.
[4] R. C. Reed, *Superalloys: Fundamentals and Applications*, Cambridge University Press, Cambridge **2006**.
[5] R. J. Quigg, *High Temp. Mater. Proc*, **1993**, *11*, 247.
[6] C. M. F. Rae, R. C. Reed, *Acta Mater*, **2001**, *49*, 4113.
[7] A. F. Giamei, D. L. Anton, *Metall. Trans. A* **1985**, *16*, 1997.
[8] T. Narita, *J. High Temp. Soc.* **2002**, *28*, 135.
[9] E. M. Slyusarenko, A. V. Peristyi, Yu. E. Kerimov, M. V. Sofin, Yu. D. Skorbov, *J. Alloys Compd.* **1998**, *264*, 180.
[10] S. Saito, K. Kurokawa, S. Hayashi, T. Takashima, T. Narita, *ECS Trans.* **2009**, *16*, 177.
[11] A. Ludwig, R. Zarnetta, S. Hamann, A. Savan, S. Thienhaus, *Int. J. Mater. Res.* **2008**, *99*, 1144.
[12] A. R. Denton, N. W. Ashcroft, *Phys. Rev. A* **1991**, *43*, 3161.
[13] A. L. Udovskii, K. K. Kadyrzhanov, T. E. Turkebaev, *Dokl. Akad. Nauk.* **1993**, *331*, 434.
[14] P. E. A. Turchi, L. Kaufman, Z. K. Liu, *CALPHAD* **2006**, *30*, 70.
[15] A. Nash, P. Nash, *Binary Alloy Phase Diagrams*, II Edn, Vol. *3* (Ed: T. B. Massalski) **1990**, 2847.
[16] A. Nash, P. Nash, *Bull. Alloy Phase Diagrams* **1985**, *6*, 348.
[17] W. Huang, Y. A. Chang, *J. Alloys Compd.* **1998**, *274*, 209.
[18] M. Palumbo, T. Abe, C. Kocer, H. Murakami, H. Onodera, *CALPHAD* **2010**, *34*, 495.
[19] Federal Institute for Materials Research and Testing, PowderCell v.2.3, http://www.ccp14.ac.uk/ccp/web-mirrors/powdcell/a_v/v_1/powder/e_cell.html.
[20] M. L. Tuganbaev, E. F. Kazakova, E. M. Sokolovskaya, *J. Less-Common Met.* **1986**, *124*, L9.
[21] C. Kittel, *Introduction to Solid State Physics*, 8th Edn. John-Wiley & Sons, New York **1956**.
[22] Y. W. Lai, S. Hamann, M. Ehmann, A. Ludwig, *Rev. Sci. Instrum.* **2011**, *82*, 063903.
[23] R. Zarnetta, Combinatorial Development and Discovery of Ternary and Quaternary Shape Memory Alloys, Ph.D. Thesis, Bochum **2010**.

